



## ORIGINAL ARTICLE

# Green synthesized silver nanoparticles destroy multidrug resistant bacteria via reactive oxygen species mediated membrane damage



Balaram Das<sup>a</sup>, Sandeep Kumar Dash<sup>a</sup>, Debasish Mandal<sup>a</sup>, Totan Ghosh<sup>b</sup>,  
Sourav Chattopadhyay<sup>a</sup>, Satyajit Tripathy<sup>a</sup>, Sabyasachi Das<sup>a</sup>,  
Sankar Kumar Dey<sup>c</sup>, Debasis Das<sup>b</sup>, Somenath Roy<sup>a,\*</sup>

<sup>a</sup> Immunology and Microbiology Laboratory, Department of Human Physiology with Community Health, Vidyasagar University, Midnapore, West Bengal 721 102, India

<sup>b</sup> Department of Chemistry, University of Calcutta, 92, A. P. C. Road, Kolkata 700 009, India

<sup>c</sup> Department of Physiology, Santal Bidroha Sardha Satabarsiki Mahavidyalaya, Goaltore, Paschim Midnapore, West Bengal 711 221, India

Received 1 May 2015; accepted 6 August 2015

Available online 21 August 2015

## KEYWORDS

Silver nanoparticles (Ag NPs);  
Green synthesis;  
Antibacterial activity;  
*Staphylococcus aureus*;  
*Escherichia coli*

**Abstract** The growing need of antimicrobial agent for novel therapies against multi-drug resistant bacteria has drawn researchers to green nanotechnology. Especially, eco-friendly biosynthesis of silver nanoparticles (Ag NPs) has shown its interesting impact against bacterial infection in laboratory research. In this study, a simple method was developed to form Ag NPs at room temperature, bio-reduction of silver ions from silver nitrate salt by leaf extract from *Ocimum gratissimum*. The Ag NPs appear to be capped with plant proteins, but are otherwise highly crystalline and pure. The Ag NPs have a zeta potential of  $-15$  mV, a hydrodynamic diameter of 31 nm with polydispersity index of 0.65, and dry sizes of  $18 \pm 3$  nm and  $16 \pm 2$  nm, based on scanning and transmission electron microscopy respectively. The minimum inhibitory concentration (MIC) of the Ag NPs against a multi-drug resistant *Escherichia coli* was  $4 \mu\text{g/mL}$  and the minimum bactericidal concentration

**Abbreviations:** Ag NPs, Silver nanoparticles; DAD, Disk agar diffusion; DLS, Dynamic light scattering; EDX, Energy-dispersive X-ray; FTIR, Fourier transform infrared spectroscopy; MBC, Minimum bactericidal concentration; MIC, Minimum inhibitory concentration; MTT, 3-(4,5-Dimethylthiazol-2-yl)-2,5-Diphenyltetrazolium Bromide; PBS, Phosphate buffer saline; SEM, Scanning electron microscopy; TEM, Transmission electron microscopy; XRD, X-ray diffraction; Rh-B, Rhodamine B

\* Corresponding author.

E-mail address: [sroy.vu@hotmail.com](mailto:sroy.vu@hotmail.com) (S. Roy).

Peer review under responsibility of King Saud University.



Production and hosting by Elsevier

(MBC) was 8 µg/mL, while the MIC and MBC against a resistant strain of *Staphylococcus aureus* were slightly higher at 8 µg/mL and 16 µg/mL respectively. Further, the Ag NPs inhibited biofilm formation by both *Escherichia coli* and *S. aureus* at concentrations similar to the MIC for each strain. Treatment of *E. coli* and *S. aureus* with Ag NPs resulted in damage to the surface of the cells and the production of reactive oxygen species. Both mechanisms likely contribute to bacterial cell death. In summary, this new method appears promising for green biosynthesis of pure Ag NPs with potent antimicrobial activity.

© 2015 The Authors. Production and hosting by Elsevier B.V. on behalf of King Saud University. This is an open access article under the CC BY-NC-ND license (<http://creativecommons.org/licenses/by-nc-nd/4.0/>).

## 1. Introduction

Different pathogenic bacteria and the antibiotic resistance by bacteria, have become a great challenge in current times. Several efforts are involved till now by the researchers in search of new antibacterial agents. In the present scenario, nano-scale materials have emerged up as novel antimicrobial agents owing to their high surface area to volume ratio and the unique chemical complexities. Nanotechnology is a rapidly growing field for the purpose of manufacturing new materials at the nano-scale level. This area is expected to open a new platform to fight and prevent disease using nanomaterials. Among the most promising nanomaterials with antibacterial properties, metallic nanoparticles became the most interesting tool (Morones et al., 2005; Albrecht et al., 2006).

Silver nanoparticles have become the focus of extensive research due to its good antimicrobial efficacy against multidrug resistant bacteria, viruses and other eukaryotic microorganisms (Gong et al., 2007). Previous studies showed that Ag NPs are capable of performing effective antibacterial property against *Staphylococcus aureus*, *Escherichia coli*, *Vibrio cholera*, *Pseudomonas aeruginosa* and *Salmonella typhi* (Morones et al., 2005; Moyer et al., 1965; Li et al., 2010). In medical treatment, silver nitrate is combined with sulfonamide to form silver sulfadiazine cream, which was used as a broad-spectrum antibacterial agent and was used for the treatment of burns. It is also highly effective against bacteria such as *E. coli*, *S. aureus*, *Klebsiella* sp., and *Pseudomonas* sp. and showed considerable antifungal and antiviral activities (Fox and Modak, 1974). These applications strongly depend on the physico-chemical properties of the produced Ag NPs such as particle size and shape, size distribution and the surface charge (Soukupov et al., 2008). Nanoparticles can be synthesized using various approaches including chemical, physical, and biological methods. Silver nanoparticles synthesized by chemical methods are toxic to different normal cells and lead to non-eco-friendly by-products which may disturb the normal cells. Ag NPs were found to exert strong acute toxic effects to various cultured cells. Only Ag NPs exposure, exhibited significant cytotoxicity at higher doses and induced abnormal cellular morphology, displaying cellular shrinkage and acquisition of an irregular shape (Kawata et al., 2009). So, an ever increasing need for environmentally friendly, non-toxic protocols for nanoparticle synthesis leads to the developing interest in biological approaches which are free from the use of toxic chemicals as by-products. Different biological aspects for

nanoparticles fabrications have been reported up to date which include bacteria (Dickson, 1999; Pum and Sleytr, 1999; Joerger et al., 2001; Nair and Pradeep, 2002), fungi (Mukherjee et al., 2001; Ahmad et al., 2003; Durán et al., 2005) and plants (Singhal et al., 2011; Huang et al., 2007; Leela and Vivekanandan, 2008; Singh et al., 2015). Due to the growing needs of eco-friendly nanoparticles, green methods are used for the synthesis of various metal nanoparticles. But recently, plant extract mediated nanoparticles fabrication proved as an advantageous way over other methods. Plant extracts mediated synthesis of nanoparticles is gaining importance due to its simplicity and eco-friendliness (Awwad and Salem, 2012). The mechanisms of NPs inhibiting bacterial growth remain unclear. It has been reported that the size and shape of NPs could affect their antibacterial activity (Zhou et al., 2012). Studies suggested four mechanisms are hypothesized for antibacterial activity and these are firstly, accumulation and dissolution of nanoparticles in the bacterial membrane changing its permeability, with subsequent release of different intracellular biomolecules and dissipation of the proton motive force across the plasma membrane (Amro et al., 2000). Second is generation of reactive oxygen species (ROSs) in the cell by NPs, with subsequent oxidative damage to cellular structures (Applerot et al., 2012). Third is uptake of nanoparticles and/or metallic ions into cells, followed by depletion of intracellular ATP production, disruption of DNA replication and DNA damage and fourth is nanoparticles and its active ions which bind with different enzymes and inactivate them, resulting in arrest of cellular respiration (Morones et al., 2005; Raffi et al., 2008; Rai et al., 2009). The nanoparticles get attached to the cell membrane and also penetrate inside the bacteria and form reactive oxygen species (ROS). The bacterial membrane contains sulfur-containing proteins and the silver nanoparticles interact with these proteins in the cell as well as with the phosphorus containing compounds such as DNA. Ag NPs destabilize plasma membrane potential and depletion of levels of intracellular ATP by targeting bacterial membrane resulting in bacterial cell death (Raffi et al., 2008; Rai et al., 2009). So, recent studies suggested that generating reactive oxygen species, damaging cellular enzymes (cellular respiratory chain), disrupting cellular membrane, and DNA damage ultimately lead to cell lysis and death.

The antibacterial activity of green synthesized Ag NPs against some drug-resistant bacteria has been established, but further investigation is needed to determine whether these particles could be an option for the treatment and prevention of drug-resistant microbial infections.

In this article, we designed rapid biosynthesis of novel Ag NPs with a simple, non-toxic, cost-effective and eco-friendly method at ambient conditions using *Ocimum gratissimum* leaf extract utilizing the reduced property of *O. gratissimum* leaves extract, which shows greater efficacy against different gram positive and gram negative bacteria even at low doses.

## 2. Materials and methods

### 2.1. Culture media and chemicals

All the microbiological media and chemicals were obtained from HiMedia Laboratories, India, Merck Ltd., SRL Pvt., Ltd., Mumbai. Ultrapure Milli Q water was used throughout the study.

### 2.2. Bacterial strains used in this study

Multidrug resistant *E. coli* (MC-2) and *S. aureus* (MMC-20) bacteria were previously isolated in our laboratory (Dash et al., 2012; Chakraborty et al., 2011). The strains were subcultured and used throughout the study. These strains are also resistant to several traditional antibiotics.

### 2.3. Preparation of the leaf extract

Leaves of *O. gratissimum* were collected from Vidyasagar University campus area, West Bengal., India. 20 g fresh leaves of *O. gratissimum* were collected and washed gently with double distilled water to remove dust particles. The leaves were finely chopped and exposed to the sun until they were completely dry. These materials were dissolved in distilled water (10 g dust/100 mL double distilled water) and filtered with Whatman filter paper No. 1. The filtrate was collected, freeze-dried and stored at 4 °C until use.

### 2.4. Synthesis and purification of Ag NPs

Synthesis of Ag NPs using dried powder of *O. gratissimum* leaf extract was done according to the method of Sintubin et al., (2011) with some modifications. Silver nanoparticles (Ag NPs) were synthesized by dissolving  $10^{-3}$  M of silver nitrate salt ( $\text{AgNO}_3$ ) in 100 mL of deionized water and this solution was placed in a 250-mL reaction vessel. A total of 100 mg freeze-dried plant leaf extract was added to the  $\text{AgNO}_3$  solution at room temperature for the bio-reduction process. After the addition of leaf extract, the pH value of the solution was immediately adjusted to 10.0 pH using a 7.7 M solution of NaOH. The reaction vessel was thereafter shaken at a rotation rate of 150 rpm in the dark condition at 30 °C for 48 h. The solution containing Ag NPs was then collected and centrifuged at 3000 rpm for 10 min for the removal of excess extract components.

### 2.5. Characterization of Ag NPs

#### 2.5.1. UV-vis spectroscopy

To observe the optical property of biosynthesized Ag NPs, samples were analyzed for UV-vis spectroscopic studies (Shimadzu UV/vis 1800 spectrophotometer) at room temperature operated at a resolution of 1 nm between 190 and 1100 nm ranges (Dash et al., 2014).

#### 2.5.2. Fourier transform infrared spectroscopy

Ag NPs were investigated by Fourier transform IR spectroscopy with a PerkinElmer Spectrum RX I Fourier transform IR system with a frequency ranging from 500 to 4000  $\text{cm}^{-1}$  and a resolution of 4  $\text{cm}^{-1}$ . The KBr pellet method was used to prepare the samples (Chattopadhyay et al., 2013a).

#### 2.5.3. Dynamic light scattering (DLS) and zeta potential

DLS analysis was done with a Zetasizer Nano ZS (Malvern Instruments) according to standard method with some modifications (Chattopadhyay et al., 2013a). The concentration of the Ag NPs was 100  $\mu\text{g}/\text{mL}$  sonicated for 2 min, and dynamic particle sizes were measured by suspending two drops of an aqueous suspension of NPs in 10 mL of Millipore water. When the NPs had completely dispersed in water, they were analyzed with a DLS analyzer. The experiments were repeated several times to obtain the average size of the NPs.

The zeta potential of the Ag NPs was measured by using a Zetasizer-Nano ZS (Malvern, Malvern Hills, U.K.). 1 mg/mL Ag NPs suspension was prepared in Milli-Q water. Then this suspension was used for the experiment (Dash et al., 2014).

#### 2.5.4. Scanning electron microscopy

The particle size and microstructure were studied by high resolution scanning electron microscopy (SEM; instrument from Nikon, Japan) (Chattopadhyay et al., 2013a). In brief, Ag NPs were suspended in deionized water at a concentration of 1 mg/mL and then sonicated using a sonicator bath until the sample forms a homogenous suspension. For size measurement, the sonicated stock solution of Ag NPs (1 mg/mL) was diluted 20 times. Then one drop of sonicated aqueous solution was taken on a glass plate and dried it. Then the sample was gold coated and images were taken. SEM was used to characterize the size and shape of Ag NPs.

#### 2.5.5. Transmission electron micrograph

The particle size and microstructure were studied by high resolution transmission electron microscopy in a JEOL 3010, Japan, operating at 200 kV according to the method of Chattopadhyay et al., (2012) with some modifications. In brief, Ag NPs were suspended in deionized water at a concentration of 1 mg/mL then the sample was sonicated using a sonicator bath until sample forms a homogenous suspension. For size measurement, sonicated stock solution of all Ag NPs (0.5 mg/mL) was diluted 20 times. TEM was used to characterize the size and shape of the Ag NPs. A drop of the aqueous Ag NPs suspension was placed on to carbon-coated copper grid and this was dried in the air to get TEM image.

#### 2.5.6. X-ray diffraction study

The solid state dispersions of Ag NPs were evaluated with X-ray powder diffraction. Diffraction patterns were obtained using an XPERT-PRO diffractometer (PANalytical Ltd., the Netherlands) with a radius of 240 mm. The  $\text{Cu K}\alpha$  radiation ( $\text{K}\alpha$  1.54060 Å) was Ni filtered. A system of diverging and receiving slits of 1° and 0.1 mm, respectively, was used. The pattern was collected with 40 kV of tube voltage and 30 mA of tube current and scanned over the  $2\theta$  range of 10–90°.

### 2.5.7. EDX study

This technique determines the elemental composition of a sample. In this study it was used to confirm the presence of silver in the particles as well as to detect the other elemental compositions of the particles. Beside identification of the elements present in the sample by the use of EDX it is also possible to estimate their concentration. The particle solution was diluted 100-fold in water and a drop of 10  $\mu$ L diluted solution was placed on a carbon stub and air-dried. The EDX spectrum was obtained at an acceleration voltage of 20 kV and collected for 19 s. Mapping was completed using pseudo-colors to represent the two-dimensional spatial distribution of energy emissions of the chemical elements present in the sample. Analysis was done using JEOL JSM 6360 equipped with an EDX (energy dispersive X-ray) analyzer (Majumdar et al., 2013).

### 2.6. Plasma protein binding assay

Plasma protein binding assay was performed by using human plasma according to Chattopadhyay et al., (2013b). Human plasma samples were collected from ten healthy individuals according to institutional bioethical approval. Two milligrams per milliliter of nanosilver was mixed with 5 mL of 50 mM PBS and 0.5 mL of human plasma (8 mg/mL) was added together and stirred vigorously within a shaking incubator for 24 h at 37 °C. The nanoparticles were centrifuged at 10,000 rpm for 10 min and supernatant was used to determine the protein concentration by following the method of Lowry et al., (1951). Plasma without NPs was used as a control to ensure that there was no protein precipitation (Lowry et al., 1951).

## 2.7. Antibacterial activity determination

### 2.7.1. MIC and MBC determination

MIC and MBC were determined by a microdilution method, using Luria broth (Hi-media, India) and inoculums of  $2.5 \times 10^5$  CFU/mL. In brief, 10  $\mu$ L ( $2.5 \times 10^5$  CFU/mL) of each bacterial strain was added individually to 1 mL of nutrient broth (NB). Different concentrations of test particles (pure suspension of particles was formed by sonication and it acts as a dissolved solution which accurately reflects the amount of silver available in solution to act on the microorganisms) were added to the test tubes containing the test strains. After 24 h of incubation, the MIC values were obtained by checking the turbidity of the bacterial growth. The MIC value corresponded to the concentration that inhibited 99% of bacterial growth (Dash et al., 2012).

The minimum bactericidal concentration (MBC) values of the particles were determined according to the standard method (Dash et al., 2012). The MBC values were determined by subculturing the MIC dilutions onto the sterile Muller Hinton agar plates incubated at 37 °C for 24 h. The lowest concentration of the nanoparticles which completely killed the tested bacteria was observed and tabulated as MBC level. The MBC value corresponded to the concentration where 100% of the bacterial growth was arrested, compared to the positive control (no treatment). All assays were performed in the Biosafety cabinet.

### 2.7.2. Tolerance level

The tolerance levels of each bacterial strain against Ag NPs were determined according to the method of May et al., (2006) using the following formula:

$$\text{Tolerance} = \text{MBC}/\text{MIC}.$$

### 2.7.3. Disk agar diffusion (DAD)

Susceptibility of different multidrug resistant bacteria to green synthesized Ag NPs was determined by the disk agar diffusion (DAD) technique according to Bauer et al., (1966). The test bacterium taken from an overnight culture (inoculated from a single colony) was freshly grown for 4 h having  $10^6$  CFU/mL standardized against McFarland's standard. With this culture, a bacterial lawn was prepared on Mueller–Hinton agar. Filter paper disks of 6-mm size were used to observe antibiotic susceptibility patterns against green synthesized Ag NPs. Silver nanoparticles and AgNO<sub>3</sub> filter paper disks were prepared by absorbing 10  $\mu$ L of 2 mg/mL Ag NPs and AgNO<sub>3</sub> solution respectively. The diameter of zone of bacterial growth inhibition surrounding the disk (including the disk) was measured (Dash et al., 2012; Bauer et al., 1966).

### 2.7.4. Killing kinetic assay

Killing kinetic assay of *E. coli* and *S. aureus* strains was studied against Ag NPs by the method of Guggenbichler et al., (1985). Bacterial growth after treatment (at their respective MBC values) was measured by quantifying cell viability at 0, 2, 4, 8, 12, 18 and 24 h after incubation with Ag NPs. The growth inhibition percentage was obtained with respect to the positive control. Bacterial cell viability was measured spectrophotometrically using Shimadzu UV/vis 1800 spectrophotometer.

### 2.7.5. Inhibition of biofilm formation

Virulence factor in terms of biofilm formation was measured according to the method of Stepanovic et al. with some modifications (Stepanovic et al., 2004). 20  $\mu$ L ( $2.5 \times 10^5$  CFU/mL) of each bacterial strain was added individually to 2 mL of nutrient broth (NB). Different concentrations of pure suspension test particles (by sonication) were added to the test tubes containing the test strains. Ag NPs treated bacterial cells were grown overnight in LB broth and then normalized to identical densities based on OD<sub>600</sub>, and 5  $\mu$ L was inoculated into 500  $\mu$ L of LB broth in 10 mL borosilicate glass tubes. The tubes were then incubated statically at 30 °C for 22 h. The tubes were rinsed with distilled water, incubated with 600  $\mu$ L of 0.1% crystal violet for 30 min, and rinsed again with distilled water. 1.0 mL of dimethyl sulphoxide was then added, the tube was vortexed and allowed to stand for 10 min, and the optical density was measured in Shimadzu UV 1800 UV/vis spectrophotometer at a wavelength of 570 nm.

### 2.7.6. Bacterial cell viability assay

Bacterial cell viability was performed after 12 h of treatment with Ag NPs by 3-(4,5-dimethylthiazol-2-yl)-2,5-diphenyltetrazolium bromide (MTT) method according to standard method (Mosmann, 1983). Drug treated bacterial cultures were centrifuged at 1000g for 10 min at 4 °C followed by repeated washing for two times with sterile PBS (pH 7.4). Thereafter, the medium was replaced with fresh RPMI (without phenol

red and FBS) containing 0.5 mg/mL of MTT. After additional 3 h incubation at 37 °C, HCl-isopropanol solution was added and after 15 min of incubation at room temperature, absorbance of solubilized MTT formazan product was measured in Shimadzu UV/vis 1800 spectrophotometer at 570 nm.

#### 2.7.7. Cell viability count by fluorescence activated cell sorter

Rh123 is stain that stains the mitochondria of living cell, here we used it as a viability stain (Mason et al., 1993b). Bacteria with membrane potential prohibit the dye to enter, but non-viable bacteria with depolarized membranes allow it to enter the cell. Cultured bacterial cells were centrifuged at 1800 rpm for 10 min at 4 °C, washed twice with Phosphate buffer saline (pH 7.4), replaced with same buffer and charged Rh123 labeled silver nanoparticles as required concentration (respective MIC concentration) and placed at 37 °C for 12 h in dark condition. Cells without Rh123 served as negative control. After incubation, cells were washed twice in PBS, and analyzed by flow cytometry (Model: FACS calibur flow cytometer, Becton Dickinson).

#### 2.7.8. Intracellular uptake study

RhB is a voltage sensitive cationic dye that is electrophoretically taken up into energized bacteria by virtue of the trans-membrane electrochemical potential (negative inside) of the plasma membrane. Ag NPs were labeled with Rhodamine B according to Mason et al. (1993). For this labeling, Rh-B dye (20 mg/mL in sterile water) was added to Ag NPs to give a concentration of 0.2 mg/mL stain and it was kept at 37 °C in darkness for 1 h. Fresh bacterial cultures were centrifuged at 1000g in 4 °C for 10 min, washed twice with PBS (pH 7.4), replaced with the same buffer and charged Rh-B labeled Ag NPs as required concentration and placed at 37 °C in darkness for 12 h. Cells without Rh-B served as negative control. After 12 h of incubation, cells were washed and re-suspended in PBS, and a drop of the suspension was examined with an Olympus research phase contrast with a fluorescence microscope (Model: CX41; Olympus Singapore Pvt., Ltd., Valley Point Office Tower, Singapore). Fluorescence images were acquired with 540 nm laser for differential interference contrast microscopy and 625 nm lasers for Rh-B excitation and emission.

#### 2.7.9. Intracellular ROS generation

The intracellular ROS production was measured by using 2,7-dichlorofluorescein diacetate (DCFH<sub>2</sub>-DA) (Dash et al., 2014). The oxidation of non-fluorescent DCFH to highly fluorescent 20,70-dichlorofluorescein (DCF) provides a quantitative assay of ROS formation. The DCFH<sub>2</sub>-DA passively enters into the cell and reacts with ROS to form the highly fluorescent compound 2,7-dichlorofluorescein. Briefly, 10 mM DCFH<sub>2</sub>-DA stock solution (in methanol) was diluted in culture medium to yield a 100 μM working solution. At the end of exposure with NPs, bacterial cells were harvested and washed three times with PBS. The cell pellet was collected and a homogeneous suspension was made by PBS up to 1 mL. Then, cells were incubated with 1.5 mL working solution of DCFH<sub>2</sub>-DA at 37 °C for 30 min. Cells were lysed in alkaline solution and centrifuged at 2200 rpm. One milliliter of supernatant was transferred to a cuvette, fluorescence was measured at 520 nm with a fluorescence spectrophotometer (Hitachi F-1700) using 485-nm excitation, and another set was prepared

in the same way for Flow cytometry analysis. The values were expressed as percent fluorescence intensity relative to control wells. Fluorescence micrographs were also taken by phase contrast microscopy. This intracellular ROS generation was confirmed by FACS analysis.

#### 2.7.10. Action of silver nanoparticles on the structures of bacterial cells

Different volumes of culture medium, Ag NPs solutions, and bacterial cells were added to 10 mL cultures resulting in final concentration of their respective MIC values and concentration of 10<sup>8</sup> CFU/mL bacterial cells. Control experiment was conducted in the absence of Ag NPs. The cultures were incubated at 37 ± 2 °C with shaking at 198 rpm for 12 h. After incubation the bacterial cultures were centrifuged and discarded the supernatants. The bacterial pallette was fixed with 50 μL of 2.5% glutaraldehyde for 5 min in 37 °C and washed three times with 1X PBS. 50 μL PBS was added to this pallet to form a suspension. One drop of fixed pallet was taken on a glass plate and dried. Then the sample was gold coated used for observation in a scanning electron microscope (SEM, Hitachi S-3000N).

#### 2.8. Statistical analysis

The data were expressed as the mean ± the standard error of the mean ( $n = 6$ ). Comparisons between the means of control and treated groups were made by one-way analysis of variance (using the statistical package Origin 6.1; Origin Lab, Northampton, MA, USA) with multiple comparison  $t$  tests, and  $p < 0.05$  is the limit of significance.

### 3. Results and discussion

#### 3.1. Synthesis of Ag NPs

After the bio-reduction process the color of the reaction vessel was darkish-brown. The appearance of a darkish-brown color

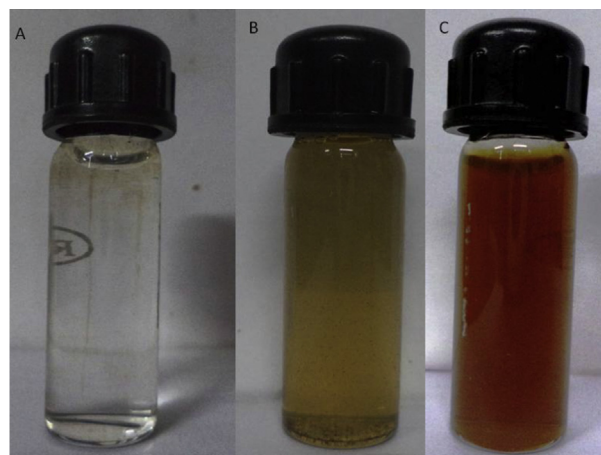


**Figure 1** Change of color indicates formation of Ag NPs. Here, A: AgNO<sub>3</sub> solution, B: AgNO<sub>3</sub> + *Ocimum gratissimum* leaf extract at 0 h, C: AgNO<sub>3</sub> + *Ocimum gratissimum* leaf extract at 48 h. Dark purple coloration indicates formation of Ag NPs.

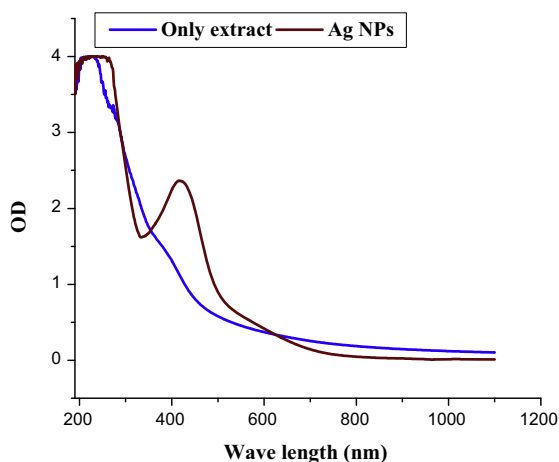


**Figure 2** UV-vis spectroscopy analysis of *Ocimum gratissimum* leaf extract and synthesized Ag NPs solution.

in reaction flasks was the indication of Ag NPs formation. The color intensity increased as a function of time due to the reduction of  $\text{Ag}^+$ . The reduction of silver ions was visibly evident from the color changes associated with it. Fig. 1 shows the only  $\text{AgNO}_3$  solution (A), the color changes before (B) and after (C) the process of reduction of the precursors as they transformed into the Ag NPs and after different aging times during its preservation under ambient conditions. After addition of the biomass to the solution of silver nitrate, the solution changed from colorless to darkish-brown. The dried biomass was found to play a crucial role in the synthesis of Ag NPs. It is well known that color change of solutions is due to excitation of surface Plasmon vibrations with the Ag NPs (Mulvaney, 1996).

### 3.2. Characterization of nanoparticles

#### 3.2.1. UV-vis spectroscopy

The absorption spectra of the Ag NPs are shown in Fig. 2. The sample showed the characteristic surface-plasmon of Ag NPs. Ag NPs had a narrow band with a maximum at 415 nm. The absorption spectrum of triangular Ag NPs showed a maximum peak between 420 and 450 nm with a blue or red shift when particle size diminished or increased, respectively (Pal et al., 2007; Jana et al., 1999).

#### 3.2.2. Fourier transform infrared spectroscopy

The FTIR measurements of green synthesized Ag NPs were carried out to identify the possible interaction between protein and Ag NPs. Results of FTIR study showed sharp absorption peaks at about  $1631$  and  $3435\text{ cm}^{-1}$  (Fig. 3). Absorption peak at  $1631\text{ cm}^{-1}$  was assigned to the amide bond of proteins arising due to the carbonyl stretch in proteins, and peaks at  $3435\text{ cm}^{-1}$  were assigned to OH stretching in alcohols and phenolic compounds. The absorption peak at  $1631\text{ cm}^{-1}$  was close to that reported for native proteins (Macdonald and Smith, 1996) which suggested that proteins were interacted with biosynthesized nanoparticles and also their secondary structure was not affected during reaction with  $\text{Ag}^+$  ions or after binding with Ag nanoparticles (Fayaz et al., 2010). The band was observed at  $1588\text{ cm}^{-1}$  due to the presence of aromatic ring and band arises at  $1452\text{ cm}^{-1}$ ,  $1383\text{ cm}^{-1}$ , and  $1349\text{ cm}^{-1}$  due to skeletal vibration of the organic substances. These IR spectroscopic studies confirmed that a carbonyl group of amino acid residue and showed a strong binding ability with metal suggested the formation of layer covering metal nanoparticles and acting as capping agent to prevent agglomeration and providing stability in the medium (Sathyavathi et al., 2010). These results confirmed the presence of possible proteins acting as reducing and stabilizing agents.

#### 3.2.3. Dynamic light scattering (DLS) and zeta potential

Average particle size, distribution and polydispersity index (PDI) of synthesized Ag NPs in solutions were evaluated by DLS technique, which are shown in Fig. 4. The DLS pattern revealed that Ag NPs synthesized by green method had a Z average diameter of  $31.45\text{ nm}$  according to the size distributions in number in percentage and  $20.53\text{ nm}$  according to the number density distribution ( $q_0$ ) by relating the number % with PDI of  $0.646$  suggesting that the nanoparticles were highly dispersive in aqueous medium. Dynamic light scattering (DLS) measures the hydrodynamic diameter of nanoparticles which is greater than actual diameter obtained from SEM and TEM images. The zeta potential value of synthesized silver nanoparticles was  $-15.2\text{ mV}$  and we assumed that Ag NPs showed good stability in water due to the electrostatic repulsion. The observed stability in combination with the measured value for the zeta potential hints for an electrosteric mechanism due to adsorption of components of the leaf extract to the particles. These organic compounds act as spacers and pre-

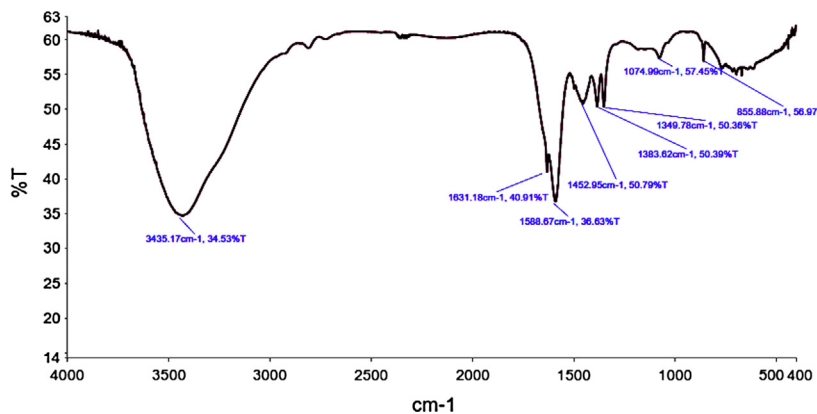


**Figure 3** Fourier transform infrared (FTIR) spectroscopy analysis of Ag NPs. KBr pallet method was applied to prepare samples.

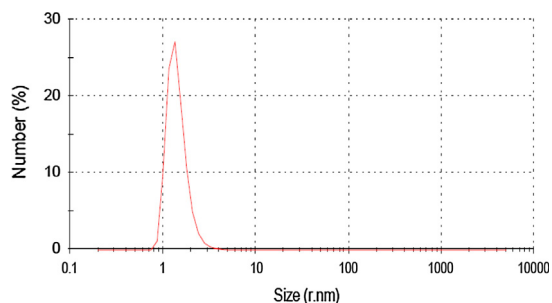


**Figure 4** The hydro-dynamic size determination of Ag NPs by dynamic light scattering (DLS) (Size Distribution Report by Number).

vent close contact between silver nanoparticles. The TEM images support the steric stabilization mechanism.

### 3.2.4. Scanning electron microscopy

The size, shape and morphology of the green synthesized Ag NPs (Ag NPs) were further characterized by SEM analysis. SEM images showed individual Ag NPs. The SEM morphology of Ag NPs showed that they had nearly triangular geometry with a mean size of  $18 \pm 3$  nm. This finding is represented in Fig. 5. The morphology of the synthesized Ag NPs by the methods was predominately triangular structure with well-defined morphology.

### 3.2.5. Transmission electron microscopy

The TEM images of the prepared Ag NPs are presented in Fig. 6. It was revealed that Ag nanoparticles were predominantly triangular in shape with maximum particles in size range with mean diameter of  $16 \pm 2$  nm and are not in physical contact with each other. It was also observed that Ag NPs were evenly distributed in the sample. The observed NP size (SEM and TEM) was slightly larger than the hydrodynamic diameter obtained from the DLS experiment. SEM or TEM describes the size in the dried state of the sample, whereas DLS measures the size in the hydrated state of the sample, so the size measured by DLS was a hydrodynamic diameter and was larger scale range (Huang et al., 2010). However, one has to bear in mind that by SEM or TEM

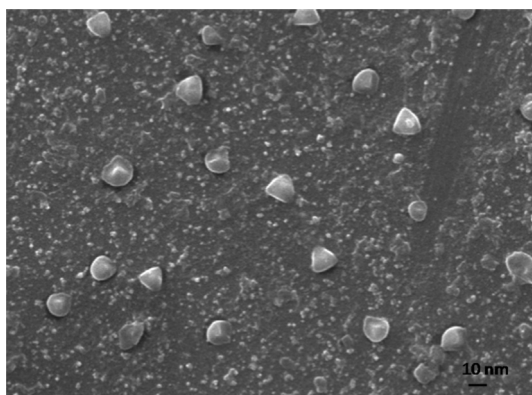


**Figure 5** Scanning electron microscopy (SEM) of synthesized Ag NPs.

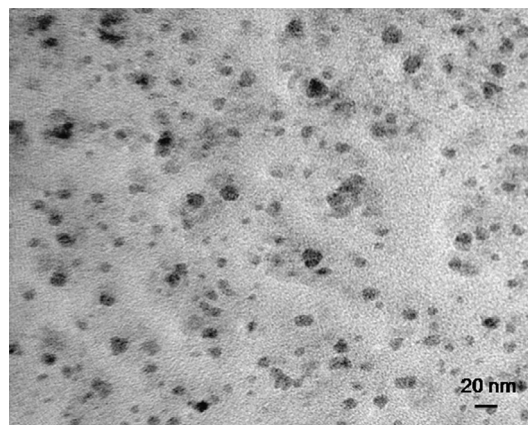


**Figure 6** Transmission electron microscopy (TEM) of synthesized Ag NPs.

analysis, we measured the image of dried particles. So, this type of differential size range was obtained. The TEM image revealed that the nanoparticles were embedded in a dense matrix which may be the organic stabilizing components of those leaf extracts.

### 3.2.6. X-ray diffraction study

The X-ray diffraction pattern of the Ag NPs synthesized by green method is shown in Fig. 7. Indexing process of powder diffraction pattern was done and Miller Indices ( $hkl$ ) to each peak are assigned in first step. No spurious diffractions were noticed due to absence of crystallographic impurities (Varshney et al., 2010). All the reflections correspond to pure silver metal with face centered cubic symmetry. The intensity of peaks reflected the high degree of crystallinity of the Ag NPs. The XRD showed that Ag NPs formed were highly crystalline in nature (Fig. 7). The data showed diffraction peaks at  $2\theta = 31.74, 45.74, 54.35, 57.04, 76.40$  and  $85.26$  which can be indexed to (100), (103), (006), (105), (008) and (203) planes of pure silver nanoparticle (JCPDS 41-1402). It confirmed that the main composition of the nanoparticles was silver. From the full width at half maximum of the X-ray diffraction peak, the crystalline size of the Ag NPs was calculated by using Scherrer equation as follows:

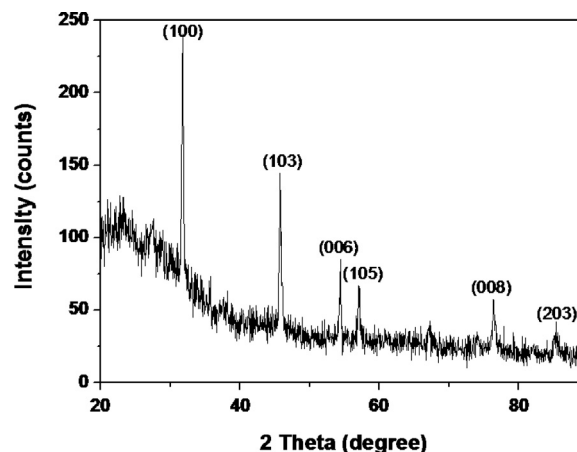


**Figure 7** X-ray diffraction (XRD) analysis of Ag NPs.

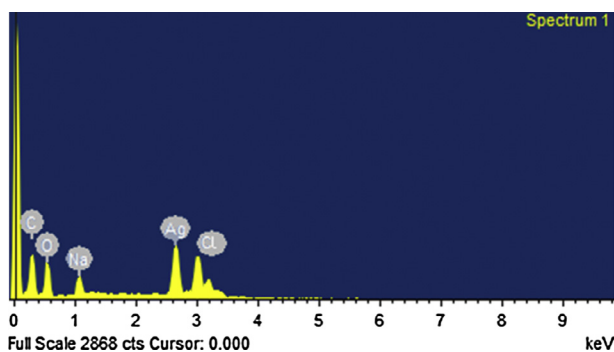


**Figure 8** Energy dispersive X-ray (EDX) spectrum of Ag NPs showing presence of different phyto-elements as capping agents.

$$B = k\lambda/\beta \cos \theta$$

where:  $B$  is the mean size of the ordered (crystalline) domains, which may be smaller or equal to the grain size;  $k$  is a dimensionless shape factor, with a value close to unity. The shape factor has a typical value of about 0.9, but varies with the actual shape of the crystallite;  $\lambda$  is the X-ray wavelength;  $\beta$  is the line broadening at half the maximum intensity (FWHM), after subtracting the instrumental line broadening, in radians. This quantity is also sometimes denoted as  $\Delta(2\theta)$ ;  $\theta$  is the Bragg angle.

The calculated sizes of Ag NPs were 20.29 nm at  $2\theta = 31.74^\circ$  and 28.93 nm at  $2\theta = 45.74^\circ$ . The particle size values derived from powder XRD plot by Scherrer equation are well matched with the particle size obtained from SEM and TEM micrograph.

The size range obtained from XRD was 20.29. As the size is too much low, the NPs must be polycrystalline, and the single crystal shows higher size range.

### 3.2.7. EDX study

Fig. 8 shows the EDX spectrum of the prepared Ag nanoparticles. Silver (Ag) signal comes from the Ag nanoparticles and the atomic percentage of silver is 31.39%. Except for Ag, there were also some other peaks. The atomic percentages of Carbon (C), Oxygen (O), Chlorine (Cl) and Sodium (Na) are 64.66%, 1.24%, 1.08% and 1.63%, respectively. The carbon (C) signal came from the adsorbed components of the leaf extract as well as coating material of the instrument. The signals of O and Cl may be due to adsorption of plant element over Ag NPs. The signal of O may partly be coming from the atmosphere or  $-\text{OH}$  from the NaOH used for pH adjustment. Sodium signal may be produced from the sodium hydroxide which was used for pH adjustment during synthesis of Ag NPs. Except carbon, other elements have a very low atomic percentage compared to silver, and suggest the formation of pure Ag NPs.

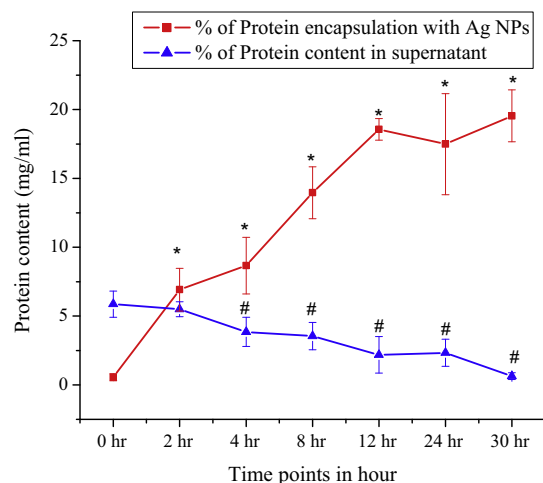


**Figure 9** Plasma protein binding assay of Ag NPs. Graph showing percentage of plasma protein binding and reduction of protein content after binding. Values are expressed as the mean  $\pm$  SEM of three experiments; superscripts indicate a significant difference ( $p < 0.05$ ) compared with the control group.

### 3.2.8. Plasma protein binding assay

The surface chemistry of nanomaterials has great effects on the protein adsorption process. Some factors such as hydrophobic interaction, electrostatic interaction, and specific chemical interactions between the protein and the adsorbent play important roles. The binding of proteins to Ag NPs is shown in Fig. 9. Our results supported that NPs can bind to different plasma proteins. The knowledge of adsorption of albumin to the NPs is very important because once in the body, blood proteins will adsorb to the particles and cells will then react with the adsorbed proteins on the particles which will ultimately affect cellular uptake and can alter biochemical activity.

## 3.3. Antibacterial activity of Ag NPs

### 3.3.1. MIC and MBC determination

Antimicrobial activity of biosynthesized Ag NPs against both gram-negative *E. coli* and gram-positive *S. aureus* microorganisms at different concentrations showed that they revealed a strong dose-dependent antimicrobial activity against both of the test microorganisms (Table 1). The antimicrobial activity (MIC and MBC) of plant extract was absent until 1024  $\mu\text{g}/\text{mL}$  against both of the bacterial strains. It was found that, as the concentration of biosynthesized nanoparticles was increased, microbial growth decreases in both the cases. Biosynthesized Ag NPs were observed to exhibit more antimicrobial activity on gram-negative microorganism than gram-positive ones. Particular drug concentration was noted where

**Table 1** MIC, MBC and DAD values of Ag NPs against multidrug resistant *E. coli* and *S. aureus* strains.

Bacterial strains	MIC ( $\mu\text{g}/\text{mL}$ )	MBC ( $\mu\text{g}/\text{mL}$ )	Tolerance (MBC/MIC ratio)	DAD (mm)
Multidrug resistant <i>Escherichia coli</i>	4	8	2	4 $\mu\text{g}/\text{mL} = 8 \pm 0.5$ 16 $\mu\text{g}/\text{mL} = 12 \pm 0.6$
Multidrug resistant <i>Staphylococcus aureus</i>	8	16	2	8 $\mu\text{g}/\text{mL} = 10 \pm 0.5$ 32 $\mu\text{g}/\text{mL} = 16 \pm 1.0$

no visible growth appears in gram positive *S. aureus* and gram negative *E. coli* broth culture in case of Ag NPs treatment. In case of gram positive *S. aureus* strain, the MIC value was 8 µg/mL, whereas in case of gram negative *E. coli* strain, the MIC value was 4 µg/mL (Table 1 and Supplementary file S1). The MIC of samples is lower when tested against *E. coli* than when tested against *S. aureus*. To avoid the possibility of misinterpretations due to the turbidity of insoluble compounds into the broth dilution tube, MBC was determined by culturing the MIC dilutions on the sterile Muller Hinton agar plates. Drug concentration was noted where no visible growth appears on agar plate in case of Ag NPs treatment. The MBC values were 16 µg/mL and 8 µg/mL in *S. aureus* and *E. coli* strain respectively when charged with Ag NPs (Table 1 and Supplementary file S2).

These results suggest that growths were inhibited due to the penetration of Ag NPs into the bacterial cell that inhibits the bacterial growth and acts as a bactericidal agent followed by bacteriostatic activity. These results can be explained on the basis of the differences in the cell wall of each strain; the cellular wall of gram-positive strains is wider than the cell wall of gram-negative strains (Thiel et al., 2007). It is well known that Gram-negative bacteria possess an outer membrane outside the peptidoglycan layer lacking in Gram-positive organisms. The important role of the outer membrane is to serve as a selective permeability barrier to protect bacteria from harmful agents, such as detergents, drugs, toxins, and degradative enzymes and penetrating nutrients to sustain bacterial growth. The structure and chemical composition of the outer membrane in *E. coli* cells have been studied extensively. The lipid bilayer of outer membrane is asymmetric: the inner leaflet mostly contains close-packed phospholipid chains, while the outer leaflet is composed of the lipopolysaccharide (LPS) molecules. Evidence from genetic and chemical experiments has proved that the LPS layer of the outer membrane plays an essential role in providing a selective permeability barrier for *E. coli* and other Gram-negative bacteria (Amro et al., 2000). Here again the cellular outer membrane plays an important role in those results.

### 3.3.2. Tolerance determination

The tolerance level of each strain against Ag NPs was calculated from the respective MIC and MBC values. In case of *S. aureus* strain, the tolerance level was 2, whereas in *E. coli* strain, the tolerance level was also 2 when charged with Ag NPs. The implication is that bactericidal agents kill microbes, whereas bacteriostatic agents simply inhibit the bacterial growth. When MBC/MIC ratio is greater than or equal to 16 for bacteria, the antimicrobial agent is considered bacteriostatic and when this ratio is less than or equal to 4, then the agent is considered bactericidal (Woods and Washington, 1995). The National Clinical Committee for Laboratory Standards (NCCLS) further suggests that an agent is bactericidal when it causes greater than a 3-log (99.9%) reduction in colony-forming units (CFU)/mL after 18–24 h of incubation in liquid media (Woods and Washington, 1995). To insure an accurate estimation of approximately 99.9% killing, the inoculum used to perform MBC analysis must be at least  $5 \times 10^5$  CFU/mL which was used during MBC test of our study. MBC is usually identical to or within 1 or 2 doubling dilutions of the MIC; if the MBC exceeds the MIC by 32-fold or more, the microbe is defined as tolerant (Woods

and Washington, 1995). The MBC/MIC ratio is a parameter that reflects the bactericidal capacity of the analyzed compound. In our study, Ag NPs exerted a bactericidal effect against the two bacterial strains because the MBC/MIC ratio values were 2. As seen in Table 1, there was no significant difference between the bactericidal effects of Ag NPs on drug-resistant microorganisms.

### 3.3.3. Disk agar diffusion (DAD)

This was evident from the values of diameter of zone of inhibition obtained during the assessment of antibacterial activity (Table 1). The zones of inhibition of *E. coli* and *S. aureus* against Ag NPs, silver nitrate and distilled water as control are shown in Supplementary file S3. For both the bacterial strains, no zone of inhibition was observed in control as well as silver nitrate solution. Bio-reduced Ag NPs showed considerable growth inhibition of two of the well-known pathogenic bacterial species. Zones of  $8 \pm 0.5$  mm and  $12 \pm 0.6$  mm were observed in *E. coli* strain on 4 µg (MIC cons.) and 8 µg (MBC cons.) of Ag NPs respectively. Zones of  $10 \pm 0.5$  mm and  $16 \pm 1$  mm were observed for *S. aureus* strain on 8 µg (MIC conc.) and 32 µg (MBC conc.) of Ag NPs respectively. Coupling of inherent property of Tulsi extract with that of Ag NPs has really proved to be beneficial to minimize the dose that needs to be administered for total microbial growth inhibition.

### 3.3.4. Killing kinetic assay

The killing kinetic assay was used to analyze post-treatment bacterial viability and to define the minimum time necessary to reach an inhibitory or bactericidal effect, since no significant difference was found between the bactericidal effects of Ag NPs on the different bacteria. The time–kill curve of Ag NPs against *E. coli* and *S. aureus* strains is presented in Fig. 10. Bactericidal activity was gradually increased to 8 h exposure of the bacteria against Ag NPs at their respective MBC concentrations for both the strains and entire bacteria were killed within this period. Ag NPs showed a time-dependent and rapid bactericidal activity against the test *E. coli* and *S. aureus* strains, and leads bacteria to early stationary phase, as shown

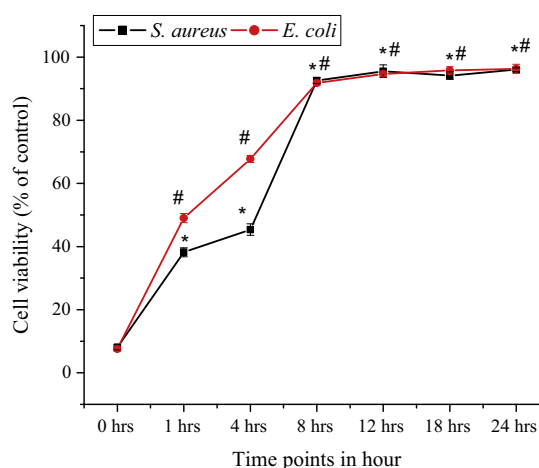


**Figure 10** Time dependent killing kinetic assay of Ag NPs against multidrug resistant *E. coli* and *S. aureus* strains. Respective MIC dose was applied to observe effective time points.

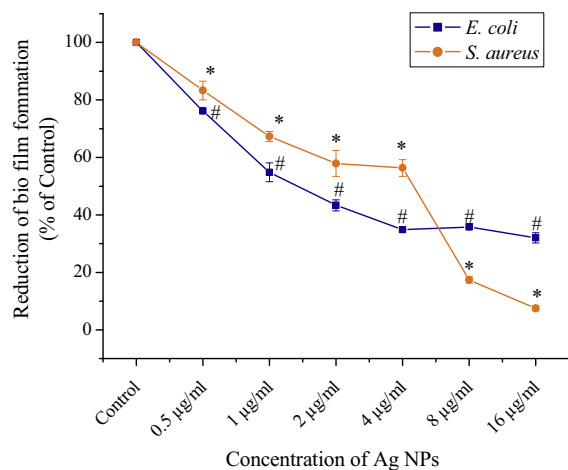


**Figure 11** Reduction of bio-film formation of multidrug resistant *E. coli* and *S. aureus* strains due to exposure of Ag NPs. Values are expressed as the mean  $\pm$  SEM of three experiments; superscripts indicate a significant difference ( $p < 0.05$ ) compared with the control group.

in time-kill curves. In our study, silver nanoparticles were effective in inhibiting bacterial growth in a dose and time dependent manner. The growth curves of bacteria exposed to Ag NPs indicated that it could inhibit the growth and reproduction of both the bacteria. Yamanaka et al. (2005) found that silver ions require about 14 h to reduce an *E. coli* population from  $10^7$  to  $10^1$  CFU/mL. As mentioned by Pal et al. (2007) the activity of nanoparticles might be similar to that of silver ions. But in the present study, after 8 h of nanoparticles treatment, the bacterial cells were killed successfully.

### 3.3.5. Inhibition of biofilm formation

Formation of biofilm begins with irreversible binding of planktonic bacteria to any surfaces. The bacteria then form a community which adheres and synthesizes extracellular matrix, and matures and disperses around the site. The results show that activity of Ag NPs is maximized or decreases biofilm formation significantly ( $p < 0.05$ ) at the concentration of 4 µg/mL, with an inhibition rate of 65.2% against *E. coli* and also in case of *S. aureus* the significant inhibition concentration was 8 µg/mL with an inhibition rate of 82.599%. It has been reported that different antimicrobial activities against planktonic bacteria could lead to different extents of biofilm inactivation by the Ag NPs. This is evident in Fig. 11. The penetration rate of the biofilm may also differ between the gram positive and the gram negative strains. The inhibition effect of Ag NPs also reduced with the increase in the bacterial cell number. The previous study has also documented that negatively charged Ag NPs can be electro-statically repulsed from the negatively charged surfaces of bacterial cells (Hong et al., 2008). This suggests that the uptake of the Ag NPs could be remarkably reduced at the rate of increase in biofilm formation. The ability of Ag NPs to agglomerate may also hinder the activity of Ag NPs. They may be less efficient in penetrating into the different extent of biofilm.

### 3.3.6. Cell viability by MTT assay and by FACS

Ag NPs significantly decreased ( $p < 0.05$ ) the cell viability of *E. coli* by 86.2% at 4 µg/mL; and 95.16% of *S. aureus* at

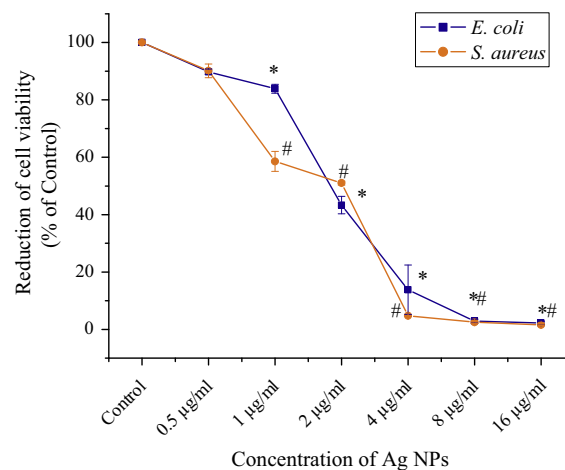


**Figure 12** Cell viability assay of Ag NPs treated multidrug resistant *E. coli* and *S. aureus* strains. Cell viability was measured by the MTT method as described in the Materials and methods. Values are expressed as the mean  $\pm$  SEM of three experiments; superscripts indicate a significant difference ( $p < 0.05$ ) compared with the control group.

8 µg/mL, which was also significant (Fig. 12). Flow cytometry and the MTT results were quite similar. Flow cytometric susceptibility test showed that silver nanoparticles slaughtered *E. coli* and *S. aureus* cells by 89.24% and 93.62%, respectively (Fig. 13). It may be due to the penetration of Ag NPs into the bacterial cell that inhibits the bacterial growth and acts as a bactericidal agent followed by bacteriostatic activity.

### 3.3.7. Intracellular uptake study

Nanoparticles binding to the plasma membrane and cellular uptake are probably a necessary condition for its exertion of activity. For assessing the Ag NPs uptake by *E. coli* and *S. aureus*, fluorescence images showed that Ag NPs treated *E. coli* and *S. aureus* cell successfully uptake the nanoparticles (Fig. 14). The uptake of silver nanoparticles was higher in *E. coli* than in the *S. aureus* strains. The Rh-B successfully labeled with Ag NPs was analyzed by FTIR spectra (Supplementary Fig. S5) which confirms Rh-B labeled Ag NPs were taken up successfully and Rh-B was not taken up independently.

Physical properties such as particle size, shape and surface charge, play a crucial role in the uptake of nanoparticles. The cellular uptake of nanoparticles was done by a two step process: first, the binding step on the cell membrane and second, the internalization step. The attachment of nanoparticles to cell membrane seems to be most affected by the surface charge of the particles. Variation of the particle surface charge could potentially control binding to the cell and direct NPs to cellular compartments. The fluorescence response to the Rh-B changes with the cell membrane potential. Bacterial cell membrane is highly electronegative and Ag NPs are comparatively less negative (nearly neutral charges). As both the bacterial cells had highly negative surface charge the Ag NPs showed maximum uptake owing to smaller size with nearly neutral surface charge, and it was also noted that the stability of the drug played another important role in cellular uptake. In the second step, the internalization of nanoparticles occurs by endocytosis pathway (Zhang et al., 2008). During endocytosis process, cells readily uptake nanomaterials by invaginating a small portion of the surface

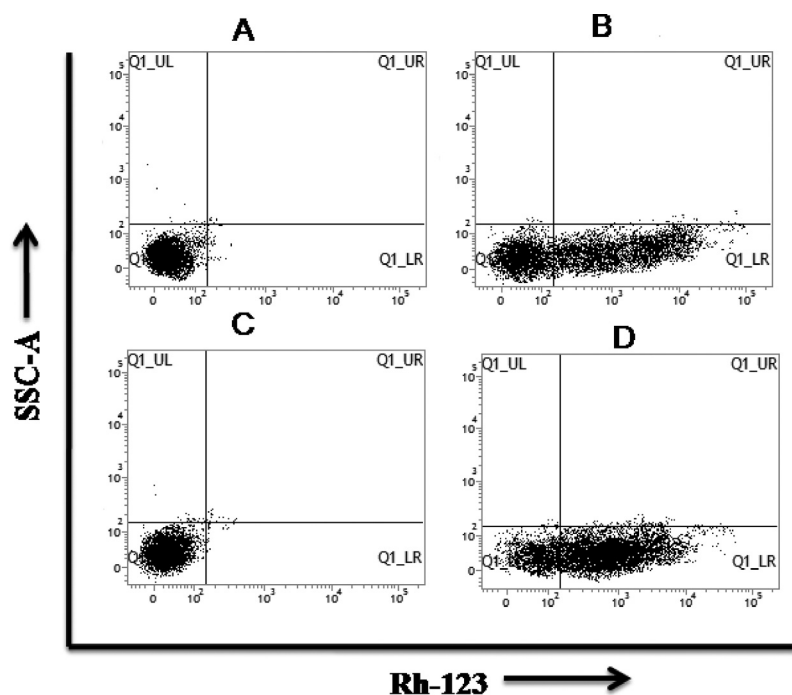


**Figure 13** Flow cytometric cell viability test of *E. coli* and *S. aureus* strains against silver nanoparticles. **A:** Control – *E. coli* without Ag NPs; **B:** Treated – *E. coli* with Ag NPs; **C:** Control – *S. aureus* without Ag NPs; **D:** Treated – *S. aureus* with Ag NPs.

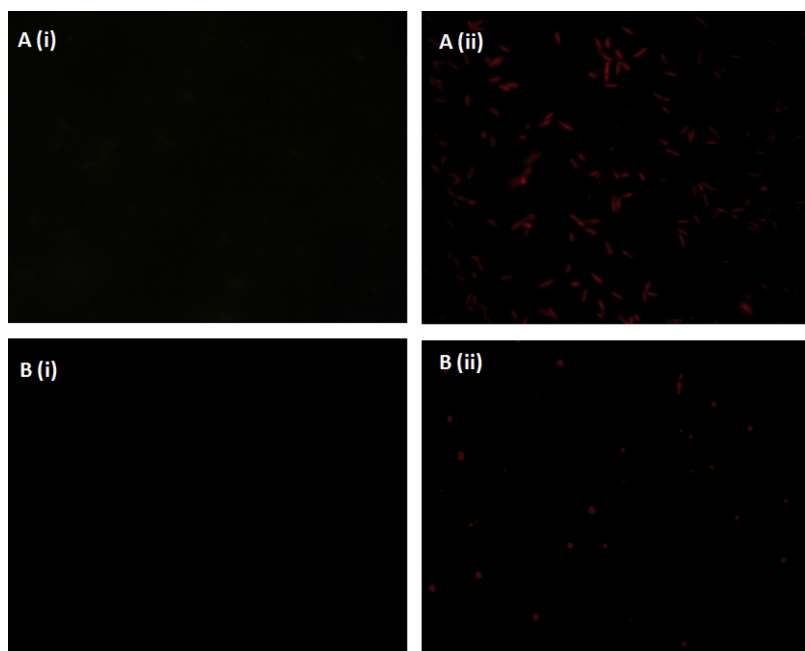


**Figure 14** Intracellular uptake of Ag NPs in multidrug resistant *E. coli* and *S. aureus* strains. A required amount of cells was treated with Rhodamine B labeled Ag NPs (2  $\mu\text{g}/\text{mL}$ ) for 4 h. Intracellular uptake was examined using a fluorescence microscope. Here, **A:** *E. coli*, **B:** *S. aureus*, (i) untreated cells and (ii): Ag NPs-Rh B treated cells.

plasma membrane and form a new intracellular vesicle around the substance to transport inside the cells (Cooper, 2000).

### 3.3.8. Intracellular ROS generation

The generation of Reactive Oxygen Species has been shown to contribute to Ag NP-triggered cytotoxicity in bacteria. In this

study, we measure the intracellular reactive oxygen species (ROS), and 2,7-dichlorofluorescein-diacetate (DCFH<sub>2</sub>-DA) was used as an intracellular ROS-indicator for the Ag NPs treated cells. After exposed to the nanoparticles, bacteria were stained with DCFH<sub>2</sub>DA for 30 min. We found that the Ag NPs treated *E. coli* and *S. aureus* bacteria became DCF+,

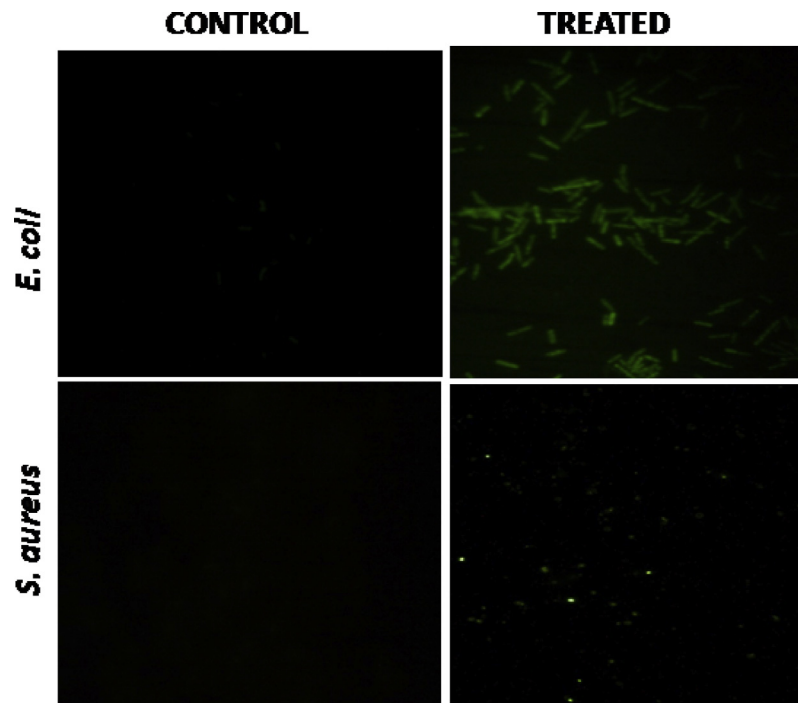


**Figure 15a** Micrographic image of intracellular ROS generation of Ag NPs in multidrug resistant *E. coli* and *S. aureus* strains.

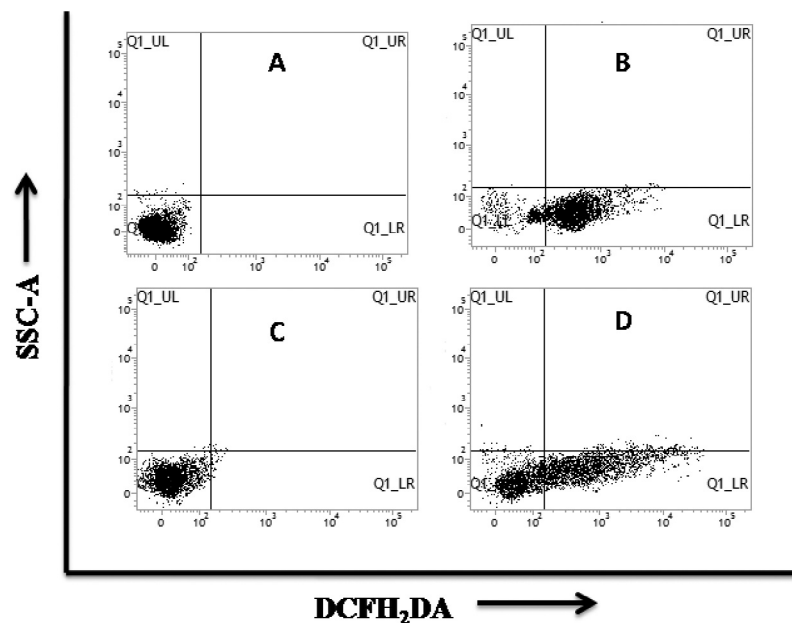


**Figure 15b** Intracellular ROS generation of Ag NPs in multidrug resistant *E. coli* and *S. aureus* strains detected by Flow cytometry. A: *E. coli* Control; B: *E. coli* treated; C: *S. aureus* Control; D: *S. aureus* Treated.

indicating that ROS were generated and participated in the Ag NPs mediated cell death (Fig. 15a). In contrast, after the same procedure without Ag NPs, no fluorescent cell was found, indicating no ROS generation. The ROS production as well as DCF fluorescence intensity was not altered significantly in both types of bacteria. Flow cytometric ROS detection showed that silver nanoparticles enhance ROS generation in *E. coli* and *S. aureus* cells by 85.68% and 89.36% respectively

(Fig. 15b). Thus, we believe that the antimicrobial ability of the Ag NPs involves the generation of intracellular ROS. Elevation of intracellular ROS levels is the main candidate mediators for the cell death. The production of ROS could be caused by the impeded electronic transport along the respiratory chain in the damaged plasma membrane (Su et al., 2009). The underlying mechanisms of ROS production in Ag NPs treated cells will be further explored in detail.

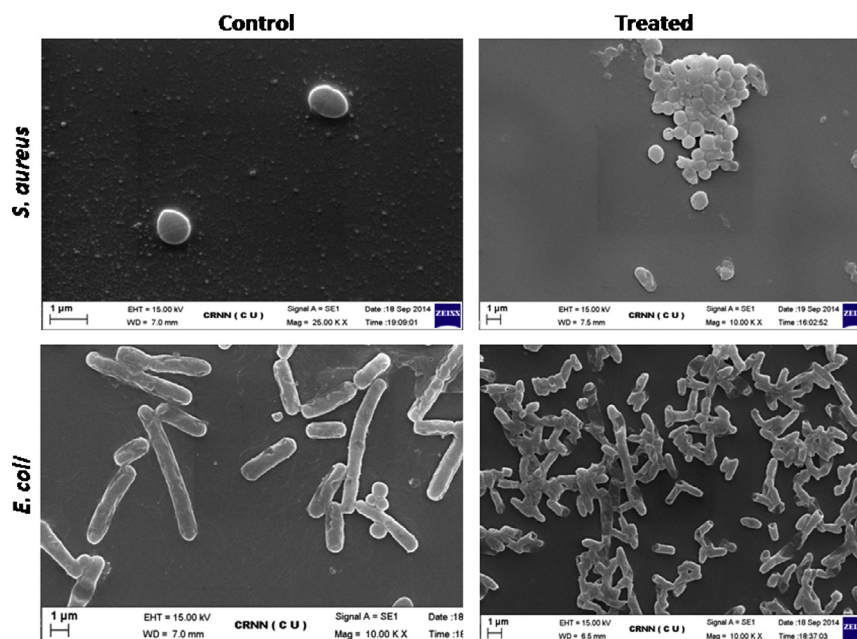


**Figure 16** Action of Ag NPs on *E. coli* and *S. aureus* cells observed by SEM. **A:** *E. coli* Control; **B:** *E. coli* treated; **C:** *S. aureus* Control; **D:** *S. aureus* Treated.

### 3.3.9. Action of silver nanoparticles on the structures of bacterial cells

The electron micrographs by SEM of *E. coli* and *S. aureus* cells treated and untreated with Ag NPs are shown in Fig. 16. Silver nanoparticles in the membrane of the bacteria as well as in its interior were observed by electron microscopy. Electron microscopy determined the distribution and location of the silver nanoparticles, as well as the morphology of the bacteria after treatment with silver nanoparticles. Micrograph by SEM showed the surface of bacterial cells of control group (untreated) was smooth and showed typical characters of surface of native cells, such as smooth and intact, and some filaments around cells were obvious, while cells treated with Ag NPs damaged severely. Some cells showed large leakage, others misshapen and fragmentary. Many pits and gaps appeared in the micrograph, and their membrane was fragmentary. The SEM micrograph of bacterial cells treated with Ag NPs showed that big gaps appeared in the cell membrane, and the bacteria were almost disorganized to several parts and show many fragmentary bacteria. The mechanism by which the nanoparticles are able to penetrate the bacteria is not understood completely, but studies suggest that when bacterial cells were treated with silver, changes took place in its membrane morphology that produced a significant increase in its permeability affecting proper transport through the plasma membrane, leaving the bacterial cells incapable of properly regulating transport through the plasma membrane, and resulting into cell death. It is observed that silver nanoparticles have penetrated inside the bacteria and have caused damage by interacting with phosphorus and sulfur containing compounds such as DNA, regulating enzymes (Morones et al., 2005). Silver tends to have a high affinity to react with such compounds. These phenomena suggest possible antibacterial mechanisms by which Ag NPs inhibit bacterial growth, as well as cellular responses to the Ag NPs treatment. Based on the present research, the action model of Ag NPs may be described as Ag NPs making a break

through the permeability of outer membrane firstly, resulting in the leakage of cellular materials. Ag NPs enter the inner membrane and produced ROS, thus inhibiting growth of cells. Simultaneously, Ag NPs may affect some cellular components to induce collapse of membrane, resulting in cell decomposition and death eventually (Li et al., 2010).

## 4. Conclusion

This study represents a successful synthesis method of Ag NPs through green route using *O. gratusimum* leaf extract as bio-reductant. Physical measurements suggested that the synthesized nanoparticles were very small in size and highly pure in nature, where plant products such as plant proteins and phytochemicals served as capping agents. The antibacterial activity of the particles was tested against multi-drug resistant *E. coli* and *S. aureus* strains. It was manifested that Ag NPs showed the anti-bacterial activity and higher effectiveness were found against *E. coli*. Ag NPs also found as an effective inhibitor of bio-film formations in both types of strains. The bacterial killing mechanism is damaging the cell membrane followed by ROS generation. This nanomaterial is another option for treatment of multidrug resistant bacterial infection. So, this biogenic Ag NPs can be applied for the treatment of superbugs in a wide aspect of medical field.

## Acknowledgments

The authors express gratefulness to the Vidyasagar University, Midnapore and CRNN, University of Calcutta for providing the facilities to execute these studies. We are heartily thankful to Mr. Joydeep Adhikari, Department of Chemistry, University of Calcutta, 92, A. P. C. Road, Kolkata - 700 009, India, for EDX measurement.

## Appendix A. Supplementary material

Supplementary data associated with this article can be found, in the online version, at <http://dx.doi.org/10.1016/j.arabj.2015.08.008>.

## References

- Ahmad, A., Senapati, S., Khan, M.I., Kumar, R., Ramani, R., Srinivas, V., Sastry, M., 2003. Intracellular synthesis of gold nanoparticles by a novel alkalotolerant actinomycete, *Rhodococcus* species. *Nanotechnology* 14, 824–828.
- Albrecht, M.A., Evan, C.W., Raston, C.L., 2006. Green chemistry and the health implications of nanoparticles. *Green Chem.* 8, 417–432.
- Amro, N.A., Kotra, L.P., Wadu-Mesthrige, K., Bulychev, A., Mobashery, S., Liu, G., 2000. High-resolution atomic force microscopy studies of the *Escherichia coli* outer membrane: structural basis for permeability. *Langmuir* 16, 2789–2796.
- Applerot, G., Lellouche, J., Lipovsky, A., Nitzan, Y., Lubar, T.R., Gedanken, A., Banin, E., 2012. Understanding the antibacterial mechanism of CuO nanoparticles: revealing the route of induced oxidative stress. *Small* 8, 3326–3337.
- Awwad, A.M., Salem, N.M., 2012. Green synthesis of silver nanoparticles by mulberry leaves extract. *Nanosci. Nanotechnol.* 2, 125–128.
- Bauer, A.W., Kirby, W.M.M., Sherris, J.C., Turch, M., 1966. Antibiotic susceptibility testing by a standardized single disk method. *Am. J. Clin. Pathol.* 45, 493–496.
- Chakraborty, S.P., KarMahapatra, S., Bal, M., Roy, S., 2011. Isolation and identification of vancomycin resistant *Staphylococcus aureus* from post operative pus sample. *Al Ameen J. Med. Sci.* 4, 152–168.
- Chattopadhyay, S., Chakraborty, S.P., Laha, D., Baral, R., Pramanik, P., Roy, S., 2012. Surface modified cobalt oxide nanoparticles: new opportunities for anti-cancer drug development. *Cancer Nano.* 3, 13–23.
- Chattopadhyay, S., Dash, S.K., Ghosh, T., Das, D., Pramanik, P., Roy, S., 2013a. Surface modification of cobalt oxide nanoparticles using phosphonomethyl iminodiacetic acid followed by folic acid: a biocompatible vehicle for targeted anticancer drug delivery. *Cancer Nano.* 4, 103–116.
- Chattopadhyay, S., Dash, S.K., Ghosh, T., Das, S., Tripathy, S., Mandal, D., Das, D., Pramanik, P., Roy, S., 2013b. Anticancer and immunostimulatory role of encapsulated tumor antigen containing cobalt oxide nanoparticles. *J. Biol. Inorg. Chem.* <http://dx.doi.org/10.1007/s00775-013-1044-y>.
- Cooper, G.M., 2000. *The Cell: A Molecular Approach*, second ed. ASM Press, Washington, DC.
- Dash, S.K., Chakraborty, S.P., Mandal, D., Roy, S., 2012. Isolation and characterization of multi drug resistant uropathogenic *Escherichia coli* from urine sample of urinary tract infected patients. *Int. J. Life Sci. Pharm. Res.* 2, ISSN: 2250-0480.
- Dash, S.K., Ghosh, T., Roy, S., Chattopadhyay, S., Das, D., 2014. Zinc sulfide nanoparticles selectively induce cytotoxic and genotoxic effects on leukemic cells: involvement of reactive oxygen species and tumor necrosis factor alpha. *J. Appl. Toxicol.* 34, 1130–1144.
- Dickson, D.P.E., 1999. Nanostructured magnetism in living systems. *J. Magn. Mater.* 203, 46–49.
- Durán, N., Marcato, P.D., Alves, O.L., De-Souza, G.I.H., Esposito, E., 2005. Mechanistic aspects of biosynthesis of silver nanoparticles by several *Fusarium oxysporum* strains. *J. Nanobiotechnol.* 3, 8.
- Fayaz, A.M., Balaji, K., Girilal, M., Yadav, R., Kalaichelvan, P.T., Venketesan, R., 2010. Biogenic synthesis of silver nanoparticles and their synergistic effect with antibiotics: a study against gram-positive and gram-negative bacteria. *Nanomed. Nanotechnol. Biol. Med.* 6, 103–109.
- Fox, C.L., Modak, S.M., 1974. Mechanism of silver sulfadiazine action on burn wound infections. *Antimicrob. Agents Chemother.* 5, 582–588.
- Gong, P., Li, H., He, X., Wang, K., Hu, J., Tan, W., Zhang, S., 2007. Preparation and antibacterial activity of Fe<sub>3</sub>O<sub>4</sub>@Ag nanoparticles. *Nanotechnology* 18, 604–611.
- Guggenbichler, J.P., Semenz, E., König, P., 1985. Kill kinetics and regrowth pattern of bacteria exposed to antibiotic concentrations simulating those observed in vivo. *J. Antimicrob. Chemother.* 15, 139–146.
- Hong, S.H., Jeong, J., Shim, S., Kang, H., Kwon, S., Ahn, K.H., Yoon, J., 2008. Effect of electric currents on bacterial detachment and inactivation. *Biotechnol. Bioeng.* 100, 379–386.
- Huang, J., Li, Q., Sun, D., Lu, Y., Su, Y., Yang, X., Wang, H., Wang, Y., Shao, W., He, N., Hong, J., Chen, C., 2007. Biosynthesis of silver and gold nanoparticles by novel sundried *Cinnamomum camphora* leaf. *Nanotechnology* 18. <http://dx.doi.org/10.1088/0957-4484/18/10/105104>.
- Huang, N.M., Lim, H.N., Radiman, S., Khiew, P.S., Chiu, W.S., Hashin, R., Chia, C.H., 2010. Sucrose ester micellar-mediated synthesis of Ag nanoparticles and the antibacterial properties. *Colloids Surf.* 353, 69–76.
- Jana, N.R., Sau, T.K., Pal, T., 1999. Growing small silver particle as redox catalyst. *J. Phys. Chem. B* 103, 115–121.
- Joerger, R., Klaus, T., Granqvist, C.G., 2001. Biologically produced silver-carbon composite materials for optically functional thin-film coating. *Adv. Mater.* 12, 407–409.
- Kawata, K., Osawa, M., Okabe, S., 2009. In vitro toxicity of silver nanoparticles at noncytotoxic doses to HepG2 human hepatoma cells. *Environ. Sci. Technol.* 43, 6046–6051.
- Leela, A., Vivekanandan, M., 2008. Tapping the unexploited plant resources for the synthesis of silver nanoparticles. *Afr. J. Biotechnol.* 7, 3162–3165.
- Li, W.R., Xie, X.B., Shi, Q.S., Zeng, H.Y., OU-Yang, Y.S., Chen, Y. B., 2010. Antibacterial activity and mechanism of silver nanoparticles on *Escherichia coli*. *Appl. Microbiol. Biotechnol.* 85, 1115–1122.
- Lowry, O.H., Rosebrough, N.J., Farr, A.L., Randall, R.J., 1951. Protein measurement with the Folin phenol reagent. *J. Biol. Chem.* 193, 265–275.
- Macdonald, I.D.G., Smith, W.E., 1996. Orientation of cytochrome c adsorbed on a citrate-reduced silver colloid surface. *Langmuir* 12, 706–713.
- Majumdar, R., Bag, B.G., Maity, N., 2013. *Acacia nilotica* (Babool) leaf extract mediated size-controlled rapid synthesis of gold nanoparticles and study of its catalytic activity. *Int. Nano Lett.* 3, 53.
- Mason, D., Allman, R., Lloyd, D., 1993. Uses of membrane potential sensitive dyes with bacteria. In: Lloyd, D. (Ed.), *Flow Cytometry in Microbiology*. Springer, London, pp. 67–82.
- May, J., Shannon, K., King, A., 2006. Glycopeptide tolerance in *Staphylococcus aureus*. *J. Antimicrob. Chemother.* 42, 189–197.
- Morones, J.R., Elechiguerra, J.L., Camacho, A., Ramirez, J.T., 2005. The bactericidal effect of silver nanoparticles. *Nanotechnology* 16, 2346–2353.
- Mosmann, T., 1983. Rapid colorimetric assay for cellular growth and survival: application to proliferation and cytotoxicity assays. *J. Immunol. Methods* 65, 55–63.
- Moyer, C.A., Brentano, L., Gravens, D.L., Margraf, H.W., Monafó Jr., W.W., 1965. Treatment of large human burns with 0.5 per cent silver nitrate solution. *Arch. Surg.* 90, 812–867.
- Mukherjee, P., Ahmad, A., Mandal, D., Senapati, S., Sainkar, S.R., Khan, M.I., Ramani, R., Parischa, R., Ajayakumar, P.V., Alam, M., Sastry, M., Kumar, R., 2001. Bioreduction of Au(Cl)<sub>4</sub>(-) ions by the fungus, *Verticillium* sp. and surface trapping of the gold nanoparticles formed. *Angew. Chem. Int. Ed. Engl.* 40, 3585–3588.
- Mulvaney, P., 1996. Surface plasmon spectroscopy of nanosized metal particles. *Langmuir* 12, 788–800.

- Nair, B., Pradeep, T., 2002. Coalescence of nanoclusters and the formation of sub-micron crystallites assisted by *Lactobacillus* strains. *Cryst. Growth Des.* 2, 293–298.
- Pal, S., Tak, Y.K., Song, J.M., 2007. Does the antibacterial activity of silver nanoparticles depend on the shape of the nanoparticle? A study of the Gram-negative bacterium *Escherichia coli*. *Appl. Environ. Microbiol.* 73, 1712–1720.
- Pum, D., Sleytr, U.B., 1999. The application of bacterial S-layers in molecular nanotechnology. *Trends Biotechnol.* 17, 8–12.
- Raffi, M., Hussain, F., Bhatti, T.M., Akhter, J.I., Hameed, A., Hasan, M.M., 2008. Antibacterial characterization of silver nanoparticles against *E. coli* ATCC-15224. *J. Mater. Sci. Technol.* 24, 192–196.
- Rai, M., Yadav, A., Gade, A., 2009. Silver nanoparticles as a new generation of antimicrobials. *Biotechnol. Adv.* 27, 76–83.
- Sathyavathi, R., Krishna, M.B., Rao, S.V., Saritha, R., Rao, D.N., 2010. Biosynthesis of silver nanoparticles using *Coriandrum sativum* leaf extract and their application in nonlinear optics. *Adv. Sci. Lett.* 3, 1–6.
- Singh, R., Shushni, M.A.M., Belkhei, A., 2015. Antibacterial and antioxidant activities of *Mentha piperita* L. *Arab. J. Chem.* 8, 322–328.
- Singhal, G., Bhavesh, R., Kasariya, K., Sharma, A.R., Singh, R.P., 2011. Biosynthesis of silver nanoparticles using *Ocimum sanctum* (Tulsi) leaf extract and screening its antimicrobial activity. *J. Nanopart. Res.* 13, 2981–2988.
- Sintubin, L., De Gussemme, B., Van der Meeren, P., Pycke, B.F., Verstraete, W., Boon, N., 2011. The antibacterial activity of biogenic silver and its mode of action. *Appl. Microbiol. Biotechnol.* 91, 153–162.
- Soukupov, J., Kvytek, L., Panacek, A., Nevecna, T., Zboril, R., 2008. Comprehensive study on surfactant role on silver nanoparticles (NPs) prepared via modified Tollens process. *Mater. Chem. Phys.* 11, 77–81.
- Stepanovic, C.S., Cirkoric, M.L., Ranin, L., Svabicviahocic, A.L., 2004. *Appl. Microbiol.* 28, 326–432.
- Su, H., Chou, C., Hung, D., Lin, S., Pao, I., Lin, J., Huang, F.L., Dong, R.X., Lin, J.J., 2009. The disruption of bacterial membrane integrity through ROS generation induced by nanohybrids of silver and clay. *Biomaterials* 30, 5979–5987.
- Thiel, J., Pakstis, L., Buzby, S., Raffi, M., Ni, C., Pochan, D.J., Shah, S.I., 2007. Antibacterial properties of silver-doped titania. *Small* 3, 799–803.
- Varshney, R., Bhadauria, S., Gaur, M.S., 2010. Biogenic synthesis of silver nanocubes and nanorods using sundried *Stevia rebaudiana* leaves. *Adv. Mater. Lett.* 1, 232–237.
- Woods, G.L., Washington, J.A., 1995. The clinician and the microbiology laboratory. In: Mandell, G., Bennett, J., Dolin, R. (Eds.), *Mandell, Douglas and Bennett's Principles and Practice of Infectious Diseases*. Churchill Livingstone, Philadelphia, PA, pp. 169–199.
- Yamanaka, M., Hara, K., Kudo, J., 2005. Bactericidal actions of a silver ion solution on *Escherichia coli*, studied by energy-filtering transmission electron microscopy and proteomic analysis. *Appl. Environ. Microbiol.* 71, 7589–7593.
- Zhang, Y., Chen, Y., Wang, T., Zhou, J., Zhao, Y., 2008. Synthesis and magnetic properties of nanoporous Co<sub>3</sub>O<sub>4</sub> nanoflowers. *Microporous Mesoporous Mater.* 114, 257–265.
- Zhou, Y., Kong, Y., Kundu, S., Cirillo, J.D., Liang, H., 2012. Antibacterial activities of gold and silver nanoparticles against *Escherichia coli* and *bacillus Calmette-Guérin*. *J. Nanobiotechnol.* 10, 19.